

Atropisomeric Effects of Second Coordination Spheres on Electrocatalytic CO₂ Reduction

Caroline K. Williams, [a] Amir Lashgari, [a] Jenny A. Tomb, [a] Jingchao Chai, [a] and Jianbing Jimmy Jiang*[a]

Control of the second coordination spheres of molecular catalytic systems has enhanced the catalytic efficiencies and facilitated the elucidation of catalytic mechanisms. Herein, we present the evaluation of stereoisomeric effects of a set of metal redox-innocent zinc porphyrin complexes on CO₂ reduction, including complexes containing four (ZnP4T) and one (ZnP1T) triazole units, and two atropisomers with two triazole units positioned at the same (ZnP2T- $\alpha\alpha$) and different (ZnP2T- $\alpha\beta$) sides of the zinc porphyrin framework. Kinetic study and

foot-of-the-wave analysis indicated that complexes with more than one triazole unit on the same side of the porphyrin framework (ZnP4T and ZnP2T- $\alpha\alpha$) display at least double maximum turnover frequency than the counterparts with a single triazole unit on the same side (**ZnP1T** and **ZnP2T**- $\alpha\beta$). These results suggest the formation of a hydrogen-bonding network in the second coordination sphere that facilitates proton transfer from the hydrophilic network to the catalyst-CO₂ intermediate.

Introduction

The conversion of carbon dioxide (CO₂) to value-added chemical feedstocks has received immense attention as an appealing strategy to mitigate energy and environmental problems. However, CO₂ is very chemically inert and thermodynamically stable, and the activation and conversion of CO_2 via multielectron/multiproton processes are kinetically restrained.[1] Therefore, much effort has been invested to develop efficient and stable catalysts to facilitate CO₂ conversion. [2] Though compelling progress has been made, most current catalysts still suffer from sluggish kinetics, low activity, and poor stability.[3] Compared to their heterogeneous counterparts, homogenous molecular catalysts are attractive because of their high catalytic selectivity and molecular tunability for uncovering the catalytic mechanism toward performance optimization.[2d,4] The most extensively studied molecular catalysts are iron porphyrins, [1d,5] rhenium bipyridine complexes, [6] iridium pincer complexes, [7] and nickel cyclams.[8]

Rational design is the first critical step toward the development of successful catalysts. Inspired by carbon monoxide (CO) dehydrogenase (CODH), which catalytically inverts CO2 and CO at near-thermodynamic potential, [9] many catalysts comprising second coordination spheres have been developed. [3a,5a,c,9a,10] The incorporated functional spheres of proton donors (phenol, amine, triazole, phosphine, imidazolium, etc.) or electrostatic sites (ammonium) stabilize the catalyst-CO₂ adduct, thus significantly decreasing the overpotential and improving the catalytic turnover numbers (TONs) and turnover frequencies (TOFs). [5c,6b,9b,10d-g,11] As an analogy to the multipoint hydrogen bonding of histidine (H_{93}) and lysine (K_{563}) in CODH, $^{[9a,11a]}$ Marinescu^[10d,11c] and Aukauloo^[11a] proposed a multi-site hydrogen bonding framework to increase catalytic activity by the facile protonation of metallocarboxylates. Dey et al. [5c,e,f,12] extensively studied iron porphyrin complexes with triazole units as the second coordination spheres. The vast majority of the reported systems are based on transition metals, where the catalytic centers undergo redox processes to facilitate catalysis. Few systems with redox-innocent centers have been reported.[1c,13]

In this work, we focused on redox-innocent zinc-centered porphyrin complexes with second coordination spheres for electrocatalytic CO₂ reduction. A set of four Zn-porphyrin complexes with different numbers and geometries of triazole units, including two atropisomers (ZnP2T- $\alpha\alpha$ and ZnP2T- $\alpha\beta$), was investigated in terms of the cooperativity effects of the second coordination sphere on catalytic efficiency. A combination of tools, including voltammetry, spectroscopy, and foot-ofthe-wave analysis (FOWA) was utilized and revealed the atropisomeric effects of the triazole units on CO₂ reduction.

Results and Discussion

The structures and synthetic route of the set of porphyrins investigated in this work are illustrated in Figure 1A. The synthesis of the catalyst, ZnP4T, commenced from the stereoisomerically pure o-tetraaminophenylporphyrins, followed by azidation and zinc metalation to afford the zinc o-azidophenylporphyrin complexes (Figure 1B). The target compound ZnP4T was prepared using a click reaction of the corresponding zinc azidoporphyrin with 1-decyne in the presence of Cu(I) in a 63% yield. The porphyrins with two triazole units on the same $(ZnP2T-\alpha\alpha)$ and opposite $(ZnP2T-\alpha\beta)$ sides of the porphyrin

Supporting information for this article is available on the WWW under https://doi.org/10.1002/cctc.202000909

[[]a] C. K. Williams, A. Lashgari, J. A. Tomb, J. Chai, J. J. Jiang Department of Chemistry University of Cincinnati P.O. Box 210172 Cincinnati, Ohio 45221-0172 (USA) E-mail: iianbina.iiana@uc.edu

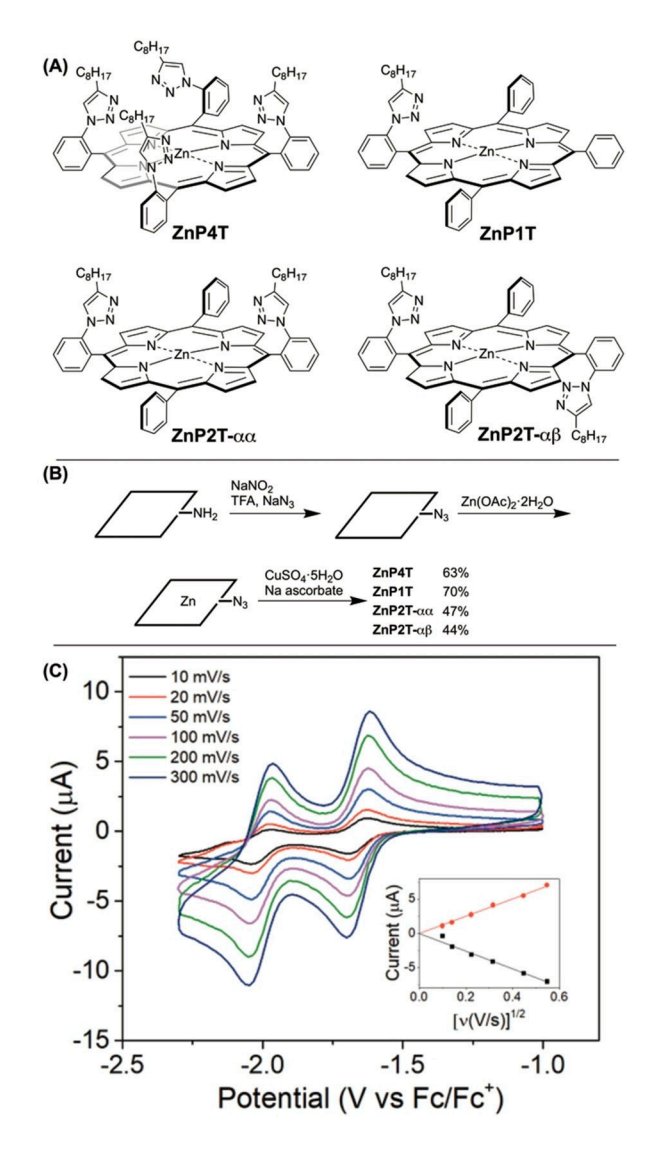


Figure 1. (A) Structures of catalysts. (B) Generic synthesis route. (C) Scanrate-dependent cyclic voltammetry of ZnP4T in DMF with 0.1 M TBAPF₆. Inset: correlation between current and square root of scan rate.

framework were also prepared starting from the corresponding atropisomerically pure o-diaminophenylporphyrins (Figure 1B). The retention of the structural configuration was confirmed by thin-layer chromatography and proton nuclear magnetic resonance (¹H NMR) spectroscopy (Figure S1) (see Supporting Information (SI) for synthesis details). All catalysts were purified

www.chemcatchem.org

and characterized by ¹H NMR, ¹³C NMR, and high-resolution mass spectrometry prior to the redox property and electrocatalysis studies.

The electrochemical properties of the catalysts were studied with CV measurements in N,N-dimethylformamide (DMF) with 0.1 M tetrabutylammonium hexafluorophosphate (TBAPF₆) containing 0.5 mM of catalyst. The ZnP4T catalyst exhibited a reversible redox couple at $-1.7 \,\mathrm{V}$ vs Fc/Fc⁺ and a quasireversible couple at -2.0 V vs Fc/Fc⁺ (Figure 1C), corresponding to two successive one-electron reduction processes on the porphyrin ligand. [13c] The other three porphyrin catalysts, ZnP1T, ZnP2T- $\alpha\alpha$, and ZnP2T- $\alpha\beta$, displayed similar redox behaviors (Figures S2-S4 and Table 1) under the same CV measurement conditions, suggesting that the incorporation of different numbers of triazole units and the geometry variation of the triazoles do not impose any significant electronic effects on the zinc porphyrin framework. To determine whether this set of Znporphyrin complexes is suitable for homogeneous catalytic studies, all catalysts were subjected to a scan-rate-dependent study. The linear relationship of the current of the first redox couple and the square root of the scan rate (Figure 1 inset and Figures S2-S4 insets) suggests diffusion-controlled processes according to the Randles-Sevcik equation.[14] The diffusion constants for all catalysts were calculated and are listed in Table 1.

The catalytic properties of the four catalysts during CO2 reduction were also investigated using CV at a scan rate of 50 mV/s. The ZnP4T catalyst in dry DMF displayed a current increase, compared to the current under the argon atmosphere due to CO₂ reduction under aprotic conditions with CO₂ as the oxygen acceptor for CO_2 -to-CO conversion (2 $CO_2 + 2e^- \rightarrow CO_3^{2-}$ +CO).[15] Greater current increase was observed at potentials more negative than -2.1 V vs Fc/Fc⁺ (Figure 2A) when water was introduced as the proton source for CO₂ reduction (CO₂+ $2H_2O + 2e^- \rightarrow CO + 2OH^-$). The same study was performed on the other three catalysts. All four Zn-porphyrins showed a similar maximum current with 2 M water (Figure 2), suggesting that the reaction order for the number of triazole units on each porphyrin (ZnP4T, ZnP2T- $\alpha\alpha$, and ZnP2T- $\alpha\beta$) is zero. This observation is distinct from a reported molecular catalytic system where the rate of catalysis shows a first-order dependence on the number of the second coordination sphere units.[10d] To gain further kinetics information, increasing scan rates were attempted to reach pure kinetic conditions in CV. [4a,16] Unfortunately, an S-shaped curve was not achieved (Figures S5-S8). Using FOWA (Equation 1) on the catalytic CV at

Table 1. Parameters of the four catalysts.					
Catalyst ^[a]	E _{1/2, 1st} [V vs Fc/Fc ⁺]	$E_{1/2, 2nd}$ [V vs Fc/Fc ⁺]	Diffusion Constant [cm²/s] ^[b]	$ \begin{array}{l} TOF_{max}^{\ \ \ \ \ \ \ \ \ \ \ \ \ \ \ \ \ \ \ $	Faradaic Efficiency ^[d]
ZnP4T	-1.7	-2.0	1.87×10^{-6} 2.16×10^{-6}	1.8×10 ⁴	99.6%
ZnP1T	-1.7	-2.1		7.9×10 ³	96.5%
ZnP2T-αα	−1.7	-2.1	6.85×10^{-7} 1.33×10^{-6}	1.1×10^4	82.1 %
ZnP2T-αβ	−1.7	-2.1		9.7×10^3	67.8 %

[a] All catalysts were prepared as 0.5 mM in DMF/0.1 M TBAPF6. [b] Derived from the Randles-Sevcik equation. [c] Derived from the foot-of-the-wave analysis. [d] At -2.3 V vs Fc/Fc+



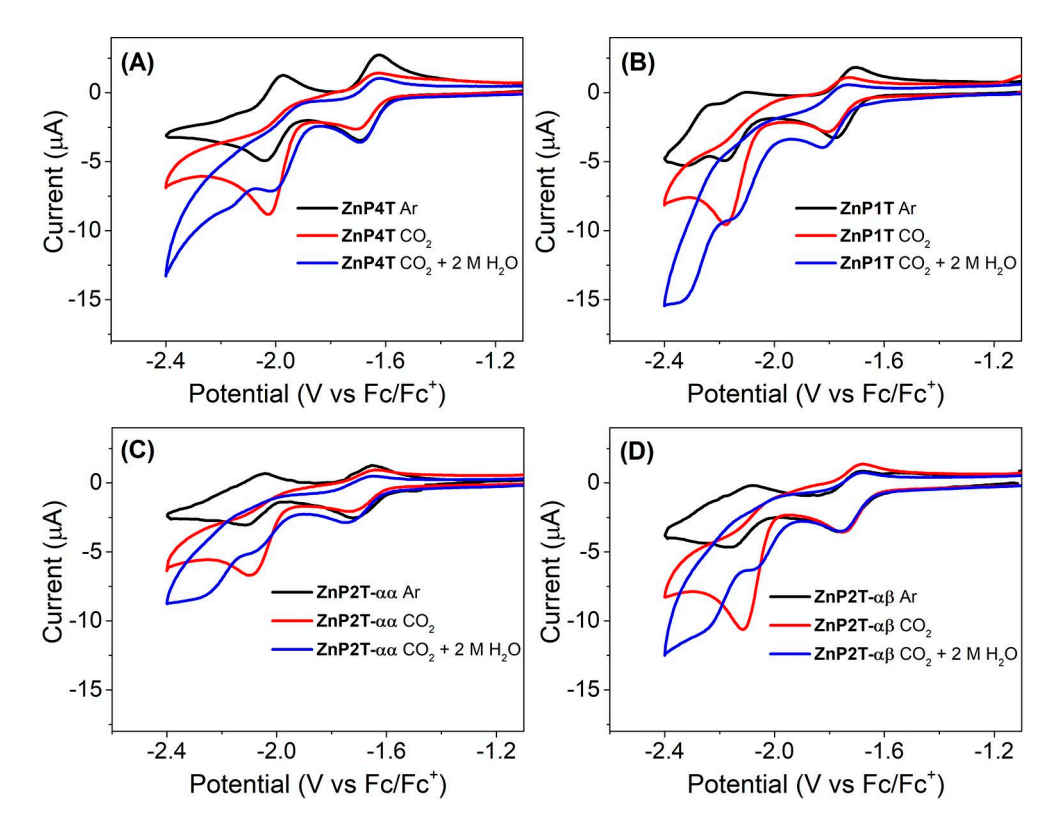


Figure 2. Cyclic voltammograms of ZnP4T (A), ZnP1T (B), ZnP2T- $\alpha\alpha$ (C), and ZnP2T- $\alpha\beta$ (D) in the presence of Ar (black), saturated CO₂ (red), and saturated CO₂ with 2 M H₂O (blue) in DMF with 0.1 M TBAPF₆ at a scan rate of 50 mV/s.

100 mV/s, the maximum turnover frequencies (TOF_{max}) of ZnP4T, ZnP1T, ZnP2T- $\alpha\alpha$, and ZnP2T- $\alpha\beta$ were calculated to be 1.8×10^4 , 7.9×10^3 , 1.1×10^4 , and 9.7×10^3 s⁻¹, respectively (Figures S9-S12). The atropisomeric complexes (ZnP2T- $\alpha\alpha$ and ZnP2T- $\alpha\beta$) showed vastly different reaction rates. Compounds with more than one triazole on the same face of the catalyst (ZnP4T and ZnP2T- $\alpha\alpha$) had reaction rates that were higher than those of the compounds with only one triazole unit per catalyst face (ZnP1T and ZnP2T- $\alpha\beta$), suggesting that the effects of the appended triazoles arise not only from the number of triazole units of the catalyst, but also from the geometry of the triazoles. It should be noted that due to the mild scale of arbitrariness for linear fitting and possible side reactions at the foot of the wave, the TOF_{max} values with close approximation are used for estimation of the catalytic efficiency.

The catalytic kinetics of $ZnP2T-\alpha\alpha$ and $ZnP2T-\alpha\beta$ on proton concentrations were studied by CV measurement with cumulative water addition, and showed distinct responses. The $ZnP2T-\alpha\alpha$ complex showed a linear increase as the water concentration increased (Figure 3A inset) which was determined using the maximum current of the catalytic wave (at – 2.4 V vs Fc/Fc⁺) divided by the current of the second redox couple under argon atmosphere (at –2.1 V vs Fc/Fc⁺). On the contrary, catalyst $ZnP2T-\alpha\beta$ showed a plateau of catalytic activity as the water content increased, and no further current increase was observed with water concentrations higher than 1 M (Figure 3B). We hypothesize that the triazole units on the same face of the porphyrin framework create a second

www.chemcatchem.org

coordination sphere effect that facilitates proton transfer to the catalyst-CO $_2$ intermediate, thus enhancing C–OH bond breakage. The **ZnP2T-** $\alpha\beta$ catalyst, with one triazole unit on each face of the porphyrin, cannot build a hydrogen-bonding network to promote CO $_2$ reduction. The same water concentration-dependent study was also performed on **ZnP4T** and **ZnP1T**, and the same catalytic responses were observed: catalyst **ZnP4T** showed a current increase as the water concentration increased (Figure S13), while catalyst **ZnP1T** behaved similarly to **ZnP2T-** $\alpha\beta$ with no distinct current increase (Figure S14). Therefore, more triazole units on the same face of the catalyst are beneficial to creating a hydrophilic environment that allows for increased catalytic activity.

Controlled-potential electrolysis (CPE) on the four catalysts was performed using carbon fiber paper as the working electrode for large-scale product generation (Figure S15). The gas product was detected by gas chromatography (Figure S16) and the possible liquid product was detected by ^1H NMR. The catalysts **ZnP4T** and **ZnP1T** started to produce CO at $-1.9\,\text{V}$ vs Fc/Fc $^+$. As more negative potentials were applied, the current densities and Faradaic efficiencies increased for both catalysts. A Faradaic efficiency of 100% at $-2.3\,\text{V}$ vs Fc/Fc $^+$ with a current density of $-4.2\,\text{mA/cm}^2$ was achieved for catalyst **ZnP4T** (Figure 4A). For catalyst **ZnP1T**, a Faradaic efficiency of 96% with a current density of $-3.0\,\text{mA/cm}^2$ at the same potential was achieved (Figure 4B). The catalysts **ZnP2T-** $\alpha\alpha$ and **ZnP2T-** $\alpha\beta$ presented maximum Faradaic efficiencies at $-2.3\,\text{V}$ vs Fc/Fc $^+$ of 82% and 68%, respectively (Figures S17 and S18), which



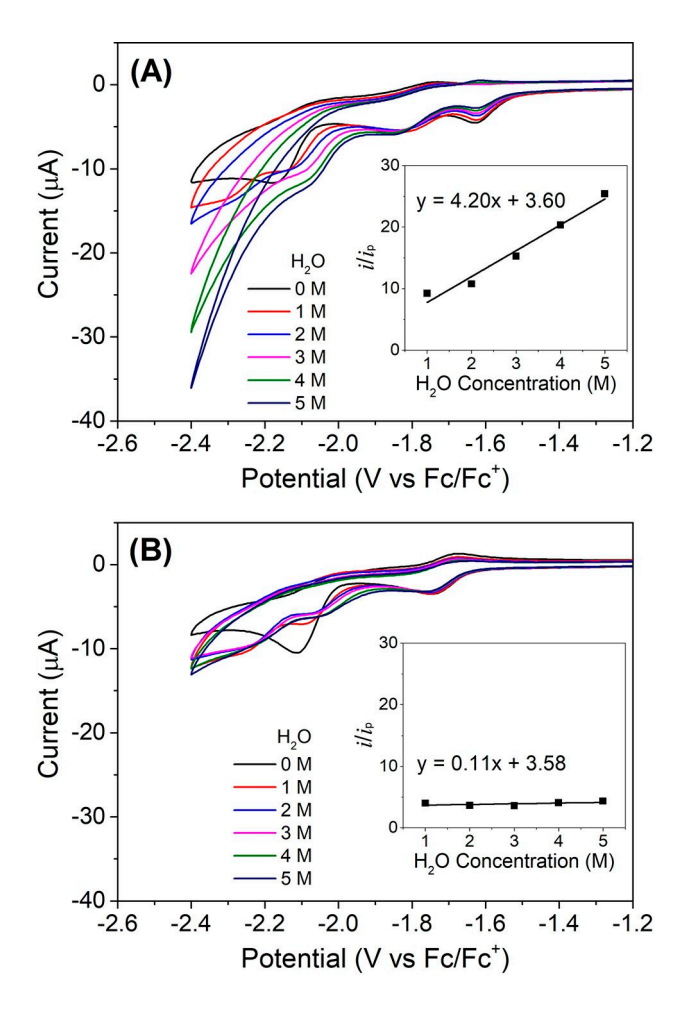


Figure 3. Cyclic voltammograms of **ZnP2T-** α α (A) and **ZnP2T-** α β (B) in DMF/ 0.1 M TBAPF₆ with increasing concentrations of water.

were presumed to be due to the instability of these two catalysts under the long-term reducing CPE conditions. All four catalysts possessed stable current density for at least two hours during the CPE experiments (Figures S19-S22). No liquid product was detected in ¹H NMR for any of the four Zn-porphyrin complexes (Figures S23-S26). A metal-free version of ZnP4T was run as a control to evaluate whether the zinc center was required for catalysis. A low Faradaic efficiency (4%) and current density (-0.2 mA/cm^2) were observed at -2.3 V vs Fc/Fc⁺ (Figure S27), suggesting that the zinc center as the binding center is critical for the reduction of CO₂.^[13c]

The stability of the four catalysts was "rinse"-tested after the CPE experiments. The carbon fiber paper electrodes were washed twice with DMF to remove any unbound molecular catalyst; CPE was then run in fresh blank electrolyte solutions. The washed electrode of **ZnP4T** presented a low current density (maximum -0.4 mA/cm^2 at -2.3 V vs Fc/Fc⁺, Figure S28), suggesting the absence of deposited elemental zinc from porphyrin demetalation, given that elemental zinc is an efficient catalyst for electrocatalytic CO₂ reduction. The mono-triazole catalyst **ZnP1T** showed similar negative CPE results (-0.3 mA/cm^2 at -2.3 V vs Fc/Fc⁺, Figure S29). The catalyst **ZnP2T-** $\alpha\alpha$

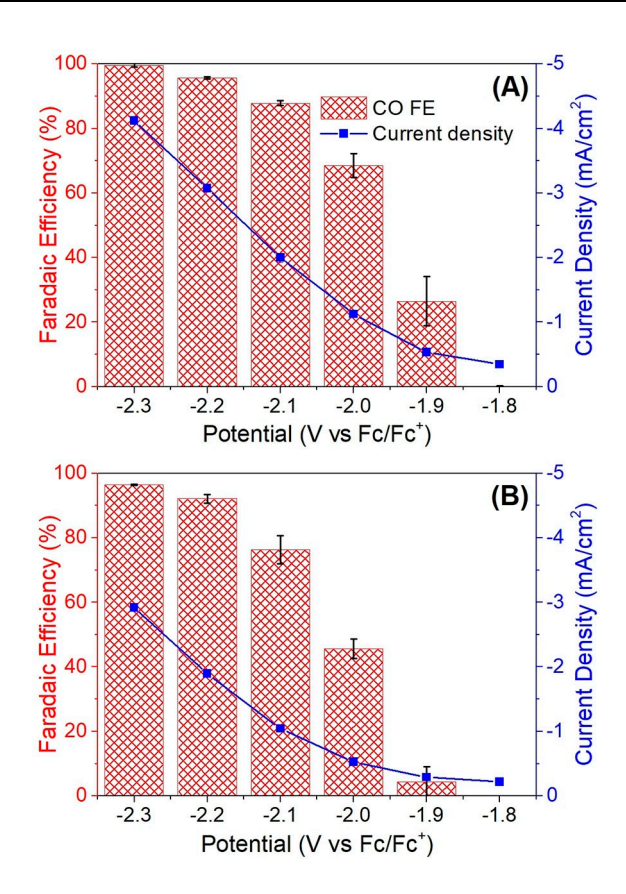


Figure 4. CO Faradaic efficiencies and current densities at various potentials for (A) **ZnP4T** and (B) **ZnP1T** in DMF with 0.1 M TBAPF $_6$ and 2 M H $_2$ O. H $_2$ gas was the only other product observed.

showed more positive results with a current density of -1.7 mA/cm^2 (Figure S30), while **ZnP2T-\alpha\beta** yielded negative CPE results as for ZnP4T and ZnP1T (Figure S31). The stability study was further investigated on the post-CPE solutions using UV-Visible spectroscopy (Figures S32-S35). The catalyst ZnP4T showed signs of an intermediate formed after CPE (Figure S32, red line), which was, presumably, hydroporphyrins originating from porphyrin ligand hydrogenation under reducing protic conditions. The hydroporphyrins are more stable than the original porphyrin and can also be catalytic active.[18] It should be noted that absorption features are observed for all four porphyrins that indicates slight demetallation. The possible partial destruction of the catalyst can be observed as a current change during the last potential of the CPE (Figures S19-S22). However, this destruction of the catalyst can be considered negligible due to the negative CPE of rinse test and the lack of Zn nanoparticles in dynamic light scattering measurements of the post electrolysis solution.

FOWA analysis of the four zinc porphyrin complexes, ZnP4T, ZnP1T, ZnP2T- $\alpha\alpha$, and ZnP2T- $\alpha\beta$, also allowed for the determination of TOF as a function of the overpotential, leading to the catalytic Tafel plot (Figure 5), where the TOF only accounts for the catalysts in the thin diffusion layer adjacent to the working electrode. The Tafel plot served to benchmark the intrinsic catalytic properties of the catalysts. The TOF/overpotential



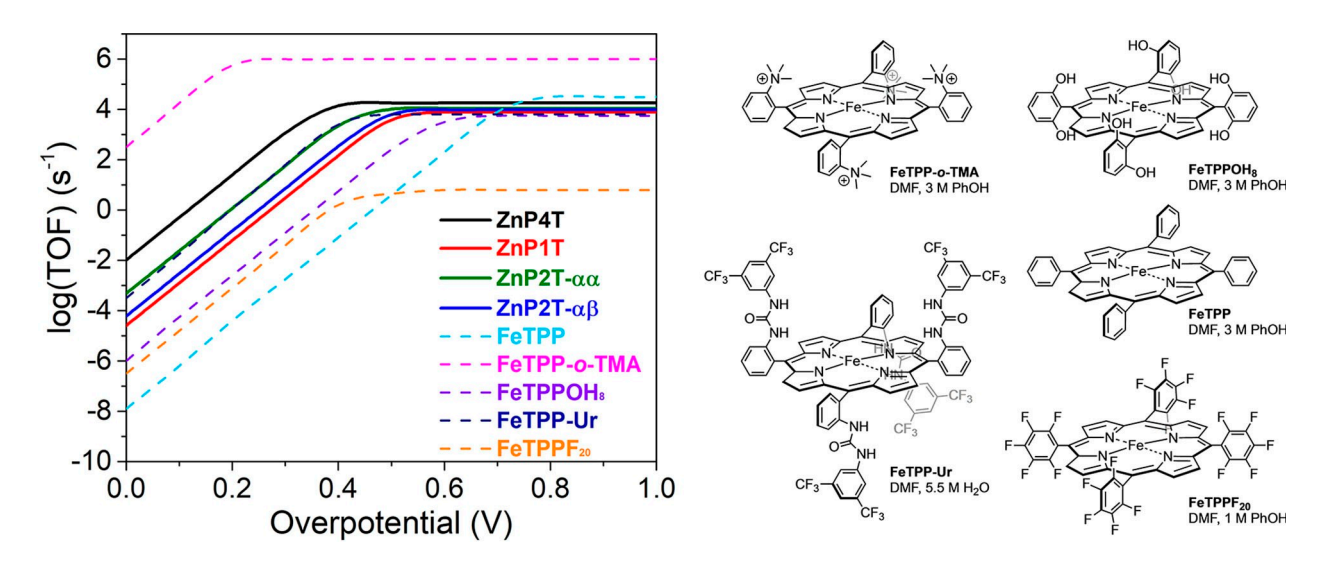


Figure 5. Tafel plots derived from cyclic voltammograms of ZnP4T, ZnP1T, ZnP2T- $\alpha\alpha$, and ZnP2T- $\alpha\beta$ in DMF with 2 M H₂O. Data for FeTPP, FeTPP-o-TMA, FeTPPOH₈, and FeTPPF₂₀ were derived from Savéant et al. [46,19] Data for FeTPP-Ur in DMF with 5.5 M H₂O were derived from Aukauloo et al. [11a]

correlation of a set of extensively studied iron porphyrins is also displayed in Figure 5 for comparison.

Conclusions

We have synthesized and evaluated the catalytic properties of four analogues of a Zn-porphyrin complex with various numbers and configurations of triazole units. The electrocatalytic CO₂ conversion study showed that all four compounds are selective to CO production. The catalyst with multiple triazoles on the same face of the Zn-porphyrin framework (ZnP4T and ZnP2T- $\alpha\alpha$) had an increased activity response to a proton source compared to the analogues where there was only one triazole moiety (ZnP1T and ZnP2T- $\alpha\beta$); this is presumably indicative of the cooperative protonation of the Znbound CO2 intermediate from the triazole bundle-promoted hydrogen-bonding network. The cooperativity design for the formation of the hydrogen-bonding network in the second coordination sphere could be extended to other protoncoupled electron transfer reactions where facile proton shuttling and subsequent protonation steps are needed.

Experimental Section

General methods

¹H NMR data were performed at room temperature with Bruker AV 400 MHz spectrometer. Chemical shifts are based on ppm unit. MALDI-TOF MS analysis was performed on a Bruker Biflex III MALDI-TOFMS instrument using 1,4-bis(5-phenyl-2-oxazolyl)benzene (PO-POP) as the matrix. Electrospray ionization-mass spectrometry (ESI-MS) analysis was performed on an Orbitrap Fusion Lumos mass spectrometer from Thermo Scientific. Compounds ZnP4Az, [5e,20] ZnP1Az,[21] and DPM[22] were prepared following reported proce-

www.chemcatchem.org

dures. All other chemical reagents were purchased from commercial sources and used as received without further purification.

Electrochemical measurements were performed using a Bio-Logic VSP potientiostat. The UV-Visible absorption spectra were obtained using an Agilent Technologies Cary 8454 UV-visible spectrometer. Any liquid products were observed via ¹H NMR using Bruker AV 400 MHz NMR. Dynamic light scattering (DLS) measurements were performed using a Microtrac Zetatrac particle size zeta potential analyzer.

Solutions of 0.5 mM catalyst in DMF with 0.1 M TBAPF₆ as the electrolyte were prepared for cyclic voltammetry in the glovebox. The CV cell was taken out of the inert atmosphere for studies with CO₂ and water. Voltammograms were collected using a glassy carbon working electrode, platinum wire counter electrode, and Ag/AgCl reference electrode. Ferrocene was added to each postcatalysis solution for potential calibration.

Controlled-potential electrolysis was performed in a split H-cell using a Selenion DSV ion-exchange membrane to separate the working and the counter cell, GDS 3250 carbon paper (Fuel Cell Store) as the working electrode, a carbon rod as the counter electrode, and a Ag/AgCl electrode as the reference electrode (Figure S15). An airtight Teflon cap was used to seal the working cell so that all gaseous products were transferred to the gas chromatograph for analysis. The gaseous products in the headspace of the cathodic chamber were injected into the sample loop of an SRI gas chromatograph equipped with a multiple gas analyzer MG#5 through the CO₂ stream. The gaseous products constantly flow to GC, and were injected for analysis twice at each potential and the obtained Faradaic efficiencies were calculated and averaged at each potential. The gas chromatograph was equipped with a 0.5-m Hayesep D column, a 2-m Molesieve column, a TCD detector (for H2 detection), a methanizer, and an FID detector (for CO detection). N₂ was used as the carrier gas. The system was calibrated with a mixture of gas calibration standards and nitrogen in various ratios for both detectors.

Post-CPE solutions were tested for liquid products by ¹H NMR using D₂O as the deuterated solvent and for demetalation/stability by UV-Visible spectroscopy. NMR samples for each catalyst were prepared by mixing 200 μL of post-electrolysis solution and 200 μL of D_2O



into a sample tube. The artifacts on the UV-Visible spectrum were manually removed.

Diffusion Constant Calculation

Using the scan rate dependent experiment and graphing the normalized current as a function of the square root of the scan rate, the linear trend of the first reduction event was then used to calculate the diffusion constants based on the Randels-Sevick equation (Equation 1). Equation 1 at constant temperature can be simplified to Equation 2.[23] The slope of the line of best fit for the normalized current vs square root of the scan rate can set to Equation 2 where diffusion constant D can be calculated. Linear fitting was set to have a y-intercept of zero according to Randles-Sevcik equation.[14a,b]

$$i_p = 0.4463 nFAC \left(\frac{nFvD}{RT}\right)^{1/2} \tag{1}$$

$$i_p = 268,600 n^{3/2} A D^{1/2} C v^{1/2}$$
 (2)

Where n is the number of electrons transferred, F is Faraday's constant, A is the surface area of the working electrode, C is the concentration in mol/cm⁻³, v is the scan rate in V/s, D is the diffusion constant in cm²/s, R is the ideal gas constant, and T is temperature in K.

FOWA Analysis

The FOWA analysis was performed following Equation 3. [4a]

$$\frac{i}{i_p} = \frac{2.24\sqrt{\frac{RT}{nFV}}\sqrt{TOF_{max}}}{1 + exp\left[\frac{nF}{nF}(E - E_{redox})\right]}$$
(3)

where $\it i$ is the catalytic current, $\it i_{\rm p}$ is the non-catalytic Faradaic current of the second redox couple, R is the universal gas constant, T is the temperature, n is the number of electron transfer processes per catalyst, F is the Faraday constant, v is the scan rate in V/s, $\mathsf{TOF}_{\mathsf{max}}$ is the maximum turnover frequency, E is the applied potential, and $\boldsymbol{E}_{\text{redox}}$ is the potential where the catalyst undergoes a mechanistic redox process in the absence of a substrate. [2d]

Thermodynamic calculation

Using pK_a values, the pK_a of H_2O in DMF is $34.7^{[24]}$ and the pK_a of carbonic acid in DMF/H₂O is 7.37.^[25] For CO₂-to-CO reduction in DMF, [26] the $E^0 = -0.73 \text{ V vs Fc}^{+/0}$ and once corrected with a pK_a of 7.37, the system has a standard thermodynamic potential for CO₂/ vs Fc^{+/0}, assuming CO of -1.17 V that there is no homoconjugation.[27]

Tafel plot calculations

TOF_{max} values were then used in the creation of the Tafel plots for each catalyst where turnover frequency (TOF) is described as a function of overpotential (η) using Equation 4. [16,28]

$$TOF \ = \frac{TOF_{max}}{1 + exp\left[\frac{F}{RT}\left(E^{\circ}_{A/B} - E_{cat/2}\right)\right]exp\left(-\frac{F}{RT}\eta\right)} \tag{4}$$

www.chemcatchem.org

Where TOF_{max} is the maximum turnover frequency calculated by FOWA analysis at 100 mV/s, F is Faraday's constant, R is the ideal gas constant, T is temperature in K, $E^{\circ}_{\ A/B}$ is the thermodynamic standard potential, E_{cat/2} is the catalytic potential of the catalyst without substrate, and η is the overpotential in V.

Acknowledgements

The authors acknowledge the University of Cincinnati for startup funding support. NMR experiments were performed on a Bruker AVANCE NEO 400 MHz NMR spectrometer funded by NSF-MRI grant CHE-1726092.

Conflict of Interest

The authors declare no conflict of interest.

Keywords: Atropisomer · Carbon Dioxide · Homogeneous Catalysis · Ligand Effects · Secondary Coordination Sphere

- [1] a) P. Kang, Z. Chen, M. Brookhart, T. J. Meyer, Top. Catal. 2014, 58, 30-45; b) W. W. Cleland, T. J. Andrews, S. Gutteridge, F. C. Hartman, G. H. Lorimer, Chem. Rev. 1998, 98, 549-562; c) E. M. Leitao, T. Jurca, I. Manners, Nat. Chem. 2013, 5, 817-829; d) C. Costentin, M. Robert, J. M. Savéant, Acc. Chem. Res. 2015, 48, 2996-3006; e) A. M. Appel, J. E. Bercaw, A. B. Bocarsly, H. Dobbek, D. L. DuBois, M. Dupuis, J. G. Ferry, E. Fujita, R. Hille, P. J. Kenis, C. A. Kerfeld, R. H. Morris, C. H. Peden, A. R. Portis, S. W. Ragsdale, T. B. Rauchfuss, J. N. Reek, L. C. Seefeldt, R. K. Thauer, G. L. Waldrop, Chem. Rev. 2013, 113, 6621-6658.
- a) M. Konig, J. Vaes, E. Klemm, D. Pant, iScience 2019, 19, 135-160; b) J. M. Barlow, J. Y. Yang, ACS Cent. Sci. 2019, 5, 580-588; c) O. R. Luca, R. H. Crabtree, Chem. Soc. Rev. 2013, 42, 1440-1459; d) R. Francke, B. Schille, M. Roemelt, Chem. Rev. 2018, 118, 4631-4701; e) A. Goeppert, M. Czaun, J. P. Jones, G. K. Surya Prakash, G. A. Olah, Chem. Soc. Rev. 2014, 43, 7995-8048; f) S. Lin, C. S. Diercks, Y. B. Zhang, N. Kornienko, E. M. Nichols, Y. Zhao, A. R. Paris, D. Kim, P. Yang, O. M. Yaghi, C. J. Chang, Science 2015, 349, 1208-1213; g) E. M. Nichols, C. J. Chang, Organometallics 2018, 38, 1213-1218; h) E. M. Nichols, J. S. Derrick, S. K. Nistanaki, P. T. Smith, C. J. Chang, Chem. Sci. 2018, 9, 2952-2960; i) B. J. McNicholas, J. D. Blakemore, A. B. Chang, C. M. Bates, W. W. Kramer, R. H. Grubbs, H. B. Gray, J. Am. Chem. Soc. 2016, 138, 11160-11163; j) P. Sen, B. Mondal, D. Saha, A. Rana, A. Dey, Dalton Trans. 2019, 48, 5965-5977; k) A. M. Cancelliere, F. Puntoriero, S. Serroni, S. Campagna, Y. Tamaki, D. Saito, O. Ishitani, Chem. Sci. 2020, 11, 1556-1563; I) H. Kumagai, T. Nishikawa, H. Koizumi, T. Yatsu, G. Sahara, Y. Yamazaki, Y. Tamaki, O. Ishitani, Chem. Sci. 2019, 10, 1597-1606; m) N. Elgrishi, M. B. Chambers, M. Fontecave, Chem. Sci. 2015, 6, 2522-2531; n) H. Jang, Y. Qiu, M. E. Hutchings, M. Nguyen, L. A. Berben, L. P. Wang, Chem. Sci. 2018, 9, 2645-2654; o) Z. Weng, J. Jiang, Y. Wu, Z. Wu, X. Guo, K. L. Materna, W. Liu, V. S. Batista, G. W. Brudvig, H. Wang, J. Am. Chem. Soc. 2016, 138, 8076-8079; p) Z. Weng, Y. Wu, M. Wang, J. Jiang, K. Yang, S. Huo, X. F. Wang, Q. Ma, G. W. Brudvig, V. S. Batista, Y. Liang, Z. Feng, H. Wang, Nat. Commun. 2018, 9, 415; q) C. I. Shaughnessy, D. J. Sconyers, T. A. Kerr, H. J. Lee, B. Subramaniam, K. C. Leonard, J. D. Blakemore, ChemSusChem 2019, 12, 3761-3768.
- [3] a) J. Rosenthal, D. G. Nocera, Acc. Chem. Res. 2007, 40, 543-553; b) J. Qiao, Y. Liu, F. Hong, J. Zhang, Chem. Soc. Rev. 2014, 43, 631-675; c) J. Schneider, H. Jia, J. T. Muckerman, E. Fujita, Chem. Soc. Rev. 2012, 41, 2036-2051; d) S. Fukuzumi, Y. M. Lee, H. S. Ahn, W. Nam, Chem. Sci. 2018, 9, 6017-6034; e) S. Sahu, D. P. Goldberg, J. Am. Chem. Soc. 2016, 138, 11410-11428.
- [4] a) E. S. Rountree, B. D. McCarthy, T. T. Eisenhart, J. L. Dempsey, Inorg. Chem. 2014, 53, 9983-10002; b) C. Costentin, G. Passard, M. Robert, J. M. Savéant, Proc. Natl. Acad. Sci. USA 2014, 111, 14990-14994.



- [5] a) C. G. Margarit, C. Schnedermann, N. G. Asimow, D. G. Nocera, Organometallics 2018, 38, 1219–1223; b) M. Abdinejad, A. Seifitokaldani, C. Dao, E. H. Sargent, X.-A. Zhang, H. B. Kraatz, ACS Appl. Energy Mater. 2019, 2, 1330–1335; c) A. Rana, B. Mondal, P. Sen, S. Dey, A. Dey, Inorg. Chem. 2017, 56, 1783–1793; d) C. T. Carver, B. D. Matson, J. M. Mayer, J. Am. Chem. Soc. 2012, 134, 5444–5447; e) S. Samanta, K. Sengupta, K. Mittra, S. Bandyopadhyay, A. Dey, Chem. Commun. 2012, 48, 7631–7633; f) B. Mondal, A. Rana, P. Sen, A. Dey, J. Am. Chem. Soc. 2015, 137, 11214–11217.
- [6] a) J. J. Teesdale, A. J. Pistner, G. P. Yap, Y. Z. Ma, D. A. Lutterman, J. Rosenthal, Catal. Today 2014, 225, 149–157; b) S. A. Chabolla, C. W. Machan, J. Yin, E. A. Dellamary, S. Sahu, N. C. Gianneschi, M. K. Gilson, F. A. Tezcan, C. P. Kubiak, Faraday Discuss. 2017, 198, 279–300; c) E. E. Benson, M. D. Sampson, K. A. Grice, J. M. Smieja, J. D. Froehlich, D. Friebel, J. A. Keith, E. A. Carter, A. Nilsson, C. P. Kubiak, Angew. Chem. Int. Ed. 2013, 52, 4841–4844; Angew. Chem. 2013, 125, 4941–4944; d) T. R. O'Toole, L. D. Margerum, T. D. Westmoreland, W. J. Vining, R. W. Murray, T. J. Meyer, J. Chem. Soc. Chem. Commun. 1985, 1416–1417; e) M. Bourrez, F. Molton, S. Chardon-Noblat, A. Deronzier, Angew. Chem. Int. Ed. 2011, 50, 9903–9906; Angew. Chem. 2011, 123, 10077–10080.
- [7] a) J. Langer, A. Hamza, I. Pápai, Angew. Chem. Int. Ed. 2018, 57, 2455–2458; Angew. Chem. 2018, 130, 2480–2483; b) S. Park, D. Bezier, M. Brookhart, J. Am. Chem. Soc. 2012, 134, 11404–11407; c) S. T. Ahn, E. A. Bielinski, E. M. Lane, Y. Chen, W. H. Bernskoetter, N. Hazari, G. T. Palmore, Chem. Commun. 2015, 51, 5947–5950; d) P. Kang, C. Cheng, Z. Chen, C. K. Schauer, T. J. Meyer, M. Brookhart, J. Am. Chem. Soc. 2012, 134, 5500–5503; e) M. Feller, U. Gellrich, A. Anaby, Y. Diskin-Posner, D. Milstein, J. Am. Chem. Soc. 2016, 138, 6445–6454.
- [8] a) K. Bujno, R. Bilewicz, L. Siegfried, T. A. Kaden, J. Electroanal. Chem.
 1998, 445, 47–53; b) J. D. Froehlich, C. P. Kubiak, Inorg. Chem. 2012, 51,
 3932–3934; c) J. Song, E. L. Klein, F. Neese, S. Ye, Inorg. Chem. 2014, 53,
 7500–7507; d) J. D. Froehlich, C. P. Kubiak, J. Am. Chem. Soc. 2015, 137,
 3565–3573.
- [9] a) J. H. Jeoung, H. Dobbek, Science 2007, 318, 1461–1464; b) S. Sung, X.
 Li, L. M. Wolf, J. R. Meeder, N. S. Bhuvanesh, K. A. Grice, J. A. Panetier, M.
 Nippe, J. Am. Chem. Soc. 2019, 141, 6569–6582.
- a) J. M. Darmon, N. Kumar, E. B. Hulley, C. J. Weiss, S. Raugei, R. M. Bullock, M. L. Helm, Chem. Sci. 2015, 6, 2737-2745; b) H. K. Ly, P. Wrzolek, N. Heidary, R. Gotz, M. Horch, J. Kozuch, M. Schwalbe, I. M. Weidinger, Chem. Sci. 2015, 6, 6999-7007; c) C. Costentin, S. Drouet, M. Robert, J. M. Savéant, Science 2012, 338, 90-94; d) A. Chapovetsky, M. Welborn, J. M. Luna, R. Haiges, T. F. Miller III, S. C. Marinescu, ACS Cent. Sci. 2018, 4, 397–404; e) M. D. Doud, K. A. Grice, A. M. Lilio, C. S. Seu, C. P. Kubiak, Organometallics 2012, 31, 779-782; f) M. L. Helm, M. P. Stewart, R. M. Bullock, M. R. DuBois, D. L. DuBois, Science 2011, 333, 863-866; g) L. Kohler, J. Niklas, R. C. Johnson, M. Zeller, O. G. Poluektov, K. L. Mulfort, Inorg. Chem. 2019, 58, 1697-1709; h) K. T. Ngo, M. McKinnon, B. Mahanti, R. Narayanan, D. C. Grills, M. Z. Ertem, J. Rochford, J. Am. Chem. Soc. 2017, 139, 2604-2618; i) K. Guo, X. Li, H. Lei, W. Zhang, R. Cao, ChemCatChem 2020, 12, 1591-1595; j) B. Zhao, H. Lei, N. Wang, G. Xu, W. Zhang, R. Cao, Chem. Eur. J. 2019, 26, 4007-4012; k) P. Gotico, Z. Halime, A. Aukauloo, *Dalton Trans.* 2020, 49, 2381–2396; l) C. G. Margarit, N. G. Asimow, M. I. Gonzalez, D. G. Nocera, J. Phys. Chem. Lett. 2020, 11, 1890-1895; m) C. K. Williams, A. Lashgari, J. Chai, J. Jiang, ChemSusChem 2020.
- [11] a) P. Gotico, B. Boitrel, R. Guillot, M. Sircoglou, A. Quaranta, Z. Halime, W. Leibl, A. Aukauloo, *Angew. Chem. Int. Ed.* **2019**, *58*, 4504–4509; b) A. Dutta, S. Lense, J. A. S. Roberts, M. L. Helm, W. J. Shaw, *Eur. J. Inorg. Chem.* **2015**, *2015*, 5218–5225; c) A. Chapovetsky, T. H. Do, R. Haiges,

- M. K. Takase, S. C. Marinescu, J. Am. Chem. Soc. 2016, 138, 5765–5768; d) E. Haviv, D. Azaiza-Dabbah, R. Carmieli, L. Avram, J. M. L. Martin, R. Neumann, J. Am. Chem. Soc. 2018, 140, 12451–12456; e) S. Sung, D. Kumar, M. Gil-Sepulcre, M. Nippe, J. Am. Chem. Soc. 2017, 139, 13993–13996; f) A. W. Nichols, C. W. Machan, Front. Chem. 2019, 7, 397; g) S. L. Hooe, J. M. Dressel, D. A. Dickie, C. W. Machan, ACS Catal. 2019, 10, 1146–1151; h) C. Jiang, A. W. Nichols, C. W. Machan, Dalton Trans. 2019, 48, 9454–9468.
- [12] B. Mondal, P. Sen, A. Rana, D. Saha, P. Das, A. Dey, ACS Catal. 2019, 9, 3895–3899.
- [13] a) A. Z. Haddad, D. Kumar, K. Ouch Sampson, A. M. Matzner, M. S. Mashuta, C. A. Grapperhaus, J. Am. Chem. Soc. 2015, 137, 9238–9241;
 b) E. J. Thompson, L. A. Berben, Angew. Chem. Int. Ed. 2015, 54, 11642–11646; Angew. Chem. 2015, 127, 11808–11812;
 c) Y. Wu, J. Jiang, Z. Weng, M. Wang, D. L. J. Broere, Y. Zhong, G. W. Brudvig, Z. Feng, H. Wang, ACS Cent. Sci. 2017, 3, 847–852.
- [14] a) J. E. B. Randles, Trans. Faraday Soc. 1948, 44, 322–327; b) J. E. B. Randles, Trans. Faraday Soc. 1948, 44, 327–338; c) A. Ševčík, Collect. Czech. Chem. Commun. 1948, 13, 349–377.
- [15] B. P. Sullivan, C. M. Bolinger, D. Conrad, W. J. Vining, T. J. Meyer, J. Chem. Soc. Chem. Commun. 1985, 1414–1416.
- [16] C. Costentin, S. Drouet, M. Robert, J. M. Savéant, J. Am. Chem. Soc. 2012, 134, 11235–11242.
- [17] a) W. Luo, J. Zhang, M. Li, A. Züttel, ACS Catal. 2019, 9, 3783–3791; b) J. Rosen, G. S. Hutchings, Q. Lu, R. V. Forest, A. Moore, F. Jiao, ACS Catal. 2015, 5, 4586–4591.
- [18] a) J. Jiang, A. J. Matula, J. R. Swierk, N. Romano, Y. Wu, V. S. Batista, R. H. Crabtree, J. S. Lindsey, H. Wang, G. W. Brudvig, ACS Catal. 2018, 8, 10131–10136; b) K. Mase, K. Ohkubo, S. Fukuzumi, J. Am. Chem. Soc. 2013, 135, 2800–2808; c) M. Taniguchi, J. S. Lindsey, Chem. Rev. 2017, 117, 344–535.
- [19] a) I. Azcarate, C. Costentin, M. Robert, J. M. Savéant, J. Am. Chem. Soc. 2016, 138, 16639–16644; b) I. Azcarate, C. Costentin, M. Robert, J.-M. Savéant, J. Phys. Chem. C 2016, 120, 28951–28960.
- [20] a) J. P. Collman, R. R. Gagne, C. A. Reed, T. R. Halbert, G. Lang, W. T. Robinson, J. Am. Chem. Soc. 1975, 97, 1427–1439; b) J. Lindsey, J. Org. Chem. 1980, 45, 5215–5215.
- [21] R. Boyle, F. Bryden, Synlett 2013, 24, 1978-1982.
- [22] C. M. Lemon, E. Karnas, M. G. Bawendi, D. G. Nocera, *Inorg. Chem.* 2013, 52, 10394–10406.
- [23] S. Roy, B. Sharma, J. Pecaut, P. Simon, M. Fontecave, P. D. Tran, E. Derat, V. Artero, J. Am. Chem. Soc. 2017, 139, 3685–3696.
- [24] W. C. Barrette, Jr., H. W. Johnson, Jr., D. T. Sawyer, Anal. Chem. 1984, 56, 1890–1898.
- [25] L. Chen, Z. Guo, X. G. Wei, C. Gallenkamp, J. Bonin, E. Anxolabehere-Mallart, K. C. Lau, T. C. Lau, M. Robert, J. Am. Chem. Soc. 2015, 137, 10918–10921.
- [26] M. L. Pegis, J. A. Roberts, D. J. Wasylenko, E. A. Mader, A. M. Appel, J. M. Mayer, *Inorg. Chem.* 2015, 54, 11883–11888.
- [27] A. M. Appel, M. L. Helm, ACS Catal. 2014, 4, 630-633.
- [28] C. Costentin, J.-M. Savéant, ChemElectroChem 2014, 1, 1226–1236.

Manuscript received: May 29, 2020 Revised manuscript received: June 21, 2020 Accepted manuscript online: June 22, 2020 Version of record online: August 10, 2020